Monthly Notices of the ROYAL ASTRONOMICAL SOCIETY
MNRAS **444,** 1660–1673 (2014) doi:10.1093/mnras/stu1537

The decomposed bulge and disc size–mass relations of massive galaxies at $1 < z < 3$ in CANDELS

V. A. Bruce,[1⋆] J. S. Dunlop,[1] R. J. McLure,[1] M. Cirasuolo,[1,2] F. Buitrago,[1] R. A. A. Bowler,[1] T. A. Targett,[3] E. F. Bell,[4] D. H. McIntosh,[5] A. Dekel,[6] S. M. Faber,[7] H. C. Ferguson,[8] N. A. Grogin,[8] W. Hartley,[9] D. D. Kocevski,[10] A. M. Koekemoer,[8] D. C. Koo[7] and E. J. McGrath[11]

[1]*SUPA† Institute for Astronomy, University of Edinburgh, Royal Observatory, Edinburgh EH9 3HJ, UK*
[2]*UK Astronomy Technology Centre, Science and Technology Facilities Council, Royal Observatory, Edinburgh EH9 3HJ, UK*
[3]*Department of Physics and Astronomy, Sonoma State University,1801 East Cotati Avenue, Rohnert Park, CA 94928-3609, USA*
[4]*Department of Astronomy, University of Michigan, Ann Arbor, MI 48109, USA*
[5]*Department of Physics and Astronomy, University of Missouri-Kansas City, 5110 Rockhill Road, Kansas City, MO 64110, USA*
[6]*Racah Institute of Physics, The Hebrew University, Jerusalem 91904, Israel*
[7]*UCO/Lick Observatory, Department of Astronomy and Astrophysics, University of California, Santa Cruz, CA 95064, USA*
[8]*Space Telescope Science Institute, 3700 San Martin Drive, Baltimore, MD 21218, USA*
[9]*ETH Zürich, Institut für Astronomie, HIT J 11.3, Wolfgang-Pauli-Str. 27, CH-8093 Zürich, Switzerland*
[10]*Department of Physics and Astronomy, University of Kentucky, Lexington, KY 40506, USA*
[11]*Department of Physics and Astronomy, Colby College, Waterville, ME 0490, USA*

Accepted 2014 July 29. Received 2014 July 29; in original form 2014 May 20

ABSTRACT

We have constructed a mass-selected sample of $M_* > 10^{11}\,M_\odot$ galaxies at $1 < z < 3$ in the CANDELS UKIDSS UDS and COSMOS fields and have decomposed these systems into their separate bulge and disc components according to their H_{160}-band morphologies. By extending this analysis to multiple bands, we have been able to conduct individual bulge and disc component SED fitting which has provided us with stellar-mass and star formation rate estimates for the separate bulge and disc components. Having utilized the new decomposed stellar-mass estimates, we confirm that the bulge components display a stronger size evolution than the discs. The median sizes of the bulge components is 3.09 ± 0.20 times smaller than similarly massive local galaxies over the full $1 < z < 3$ redshift range; for the discs, the corresponding factor is 1.77 ± 0.10. Moreover, by splitting our sample into the passive and star-forming bulge and disc sub-populations and examining their sizes as a fraction of their present-day counter-parts, we find that the star-forming and passive bulges are equally compact, star-forming discs are larger, while the passive discs have intermediate sizes. This trend is not evident when classifying galaxy morphology on the basis of single-Sérsic fits and adopting the overall star formation rates. Finally, by evolving the star formation histories of the passive discs back to the redshifts when the passive discs were last active, we show that the passive and star-forming discs have consistent sizes at the relevant epoch. These trends need to be reproduced by any mechanisms which attempt to explain the morphological evolution of galaxies.

Key words: galaxies: elliptical and lenticular, cD – galaxies: evolution – galaxies: high-redshift – galaxies: spiral – galaxies: structure.

1 INTRODUCTION

In recent years, increasingly detailed high-resolution morphological studies of massive galaxies at $z > 1$ have provided strong evidence for evolution in the sizes of high-redshift galaxies, which are observed to be up to a factor of ∼2–6 (e.g. Daddi et al. 2005; Trujillo et al. 2006; Toft et al. 2007; Trujillo et al. 2007; Buitrago et al. 2008; Cimatti et al. 2008; Franx et al. 2008; van Dokkum et al. 2008; Damjanov et al. 2009 and Cassata et al. 2010) more compact than similarly massive present-day systems, with the most compact high-redshift systems also being seen to be the most passive

⋆E-mail: vab@roe.ac.uk
† Scottish Universities Physics Alliance

(Toft et al. 2007; Kriek et al. 2009; Newman et al. 2012; McLure et al. 2013).

Despite early suggestions that the sizes of these systems were underpredicted due to selection effects and measurement uncertainties in both mass and size (Muzzin et al. 2009; van der Wel et al. 2009; Mancini et al. 2010), several spectroscopic campaigns (van der Wel et al. 2008; Newman et al. 2010; van de Sande et al. 2011, 2013; McLure et al. 2013) have subsequently provided more robust dynamical mass measurements. Additionally, tests of the sizes of simulated galaxies recovered by commonly adopted fitting procedures, such as GALFIT (Peng et al. 2010) and GALAPAGOS (Barden et al. 2012), by Häussler et al. (2007), van der Wel et al. (2012), Newman et al. (2012), and more recently by Davari et al. (2014) for more complex morphological systems equivalent to local ellipticals, have shown that these size estimates are not significantly biased or underestimated. These results, coupled with the deep morphological studies of small samples by Szomoru et al. (2010), Szomoru, Franx & van Dokkum (2012) and Trujillo, Carrasco & Ferré-Mateu (2012) confirm the genuine compactness of high-redshift galaxies.

However, in spite of mounting evidence for the evolution in the median size of the massive galaxy population with redshift, there remains debate over whether a significant fraction of the compact systems survive to the present day and, moreover, if the increase in the median size of galaxies is driven by the growth of individual systems or by the addition of newly quenched, larger, galaxies to the passive population.

Recent studies such as those by Valentinuzzi et al. (2010a) and Poggianti et al. (2013a) for cluster and field environments, respectively, have found that a significant fraction of local systems ($\sim$20 per cent) are compact. These results, coupled with comoving number density redshift evolution studies of compact, passive galaxies (Cassata et al. 2011, 2013; Carollo et al. 2013; Poggianti et al. 2013b), and the associated suggestions that the reported size evolution of massive galaxies may be overestimated due to the effects of progenitor bias, have argued that the observed evolution in the median sizes of the massive galaxy population may not be primarily driven by the growth of individual systems (e.g. via minor merging or adiabatic expansion as proposed by Khochfar & Silk 2006; Naab et al. 2007; Fan et al. 2008, 2010; Hopkins et al. 2009; Shankar et al. 2011), but instead by the addition of newly quenched, larger, galaxies to this population with time (Carollo et al. 2013; Krogager et al. 2013; Poggianti et al. 2013b).

However, the newly reported prevalence of low-redshift compact galaxies is in conflict with previous studies with Sloan Digital Sky Survey (SDSS), which found that as little as $\sim$0.03 per cent of the local population can be classified as compact (Trujillo et al. 2009; Taylor et al. 2010). Moreover, the latest comoving number density study of passive early-type galaxies (ETGs) over $0 < z < 3$ within the full Cosmic Assembly Near-infrared Deep Extragalactic Legacy Survey (CANDELS) + 3D-*HST* fields by van der Wel et al. (2014) shows that, whilst the overall comoving number density of 'compact' systems (defined simply as $r_e < 2$ kpc) does not appear to evolve strongly with redshift, the size distribution of galaxies within this 'compact' classification does, such that the comoving number density of small galaxies decreases with decreasing redshift. In addition to this, there is new evidence provided by the $z > 1$ velocity dispersion study of Belli, Newman & Ellis (2014), which reveals that by accounting for progenitor bias by considering systems at fixed velocity dispersions with redshift, the dominant contribution to the growth in sizes of passive galaxies within the range $0 < z < 2$ is the increase in the size of individual systems, rather than the addition of newly quenched, larger galaxies.

Existing studies of galaxy size evolution at $z > 1$ have almost exclusively been conducted by fitting single-Sérsic light profiles to galaxies in order to measure their effective radii. However, it is becoming increasingly clear that within the $1 < z < 3$ regime massive galaxies are undergoing dramatic structural transformations from disc-dominated and visually disturbed morphological systems at $z > 2$ to bulge dominated at lower redshifts (van der Wel et al. 2011; Bruce et al. 2012; Wuyts et al. 2012; Buitrago et al. 2013; McLure et al. 2013; Mortlock et al. 2013; Mozena et al. 2013). Therefore, in order to best conduct the studies of the morphological evolution of galaxies at high redshift, it is vital to trace both the bulge and disc components separately by decomposing galaxy morphologies into these two components. Previously, such bulge-disc decompositions have generally been conducted in the local Universe (e.g. de Jong 1996; Allen et al. 2006; Cameron et al. 2009; Simard et al. 2011 and Lackner & Gunn 2012), where high-resolution imaging is more readily available. By contrast, bulge-disc decompositions at high redshifts have been limited to small samples (van der Wel et al. 2011). However, with the advent of large, high-resolution surveys such as CANDELS with *Hubble Space Telescope* (*HST*) Wide Field Camera 3 (WFC3), it is now possible to conduct the first decompositions at rest-frame wavelengths longer than the 4000 Å break (tracing the assembled stellar mass) for statistically significant mass-selected samples of high-redshift galaxies (Bruce et al. 2012 and also Lang et al. 2014, who conduct similar decompositions on stellar-mass maps). The results from our previous analysis (Bruce et al. 2012) explicitly revealed that the bulge components display a much stronger size evolution with redshift than the disc components. However, this study was limited by the use of stellar-mass estimates determined for the entire galaxy which were sub-divided for the bulge and disc components based purely on the fraction of the H_{160}-band light which was attributed to each component. In the new study presented here, we have further utilized the bulge-disc morphological decomposition approach to extend our analysis to the additional three photometric bands covered by CANDELS in order to conduct separate-component spectral energy distribution (SED) fitting. As described in Bruce et al. (2014), this analysis has allowed separate stellar masses and, additionally, star formation rates to be estimated for the individual bulge and disc components. Here, we use this new information to explore the size evolution of the bulge and disc components by separating them into star-forming and passive sub-populations based on their specific star formation rates.

The structure of this paper is as follows. In Section 2, we provide a summary of our data sets and the sample properties. This is followed in Section 3 by a brief overview of our decomposed multi-band morphological fitting and SED fitting procedure. In Section 4, we present the results from our analysis and explore the relation between single-Sérsic index fits and bulge-to-total light fractions, the decomposed size–mass relations of the galaxies in our sample and any trends with decomposed star formation rates. We also use our decompositions to probe the fractional size evolutional of galaxies split into the decomposed disc and bulge, passive and star-forming sub-samples. These results are compared to those from existing studies in Section 5, after which we conclude with a discussion of our findings within the context of current galaxy size growth and quenching models. Finally, in Section 6 we summarize our main results.

Throughout this work, we quote magnitudes in the AB system, and calculate all physical quantities assuming a Λ cold dark matter (Λ CDM) universe with $\Omega_m = 0.3$, $\Omega_\Lambda = 0.7$ and $H_0 = 70\,\mathrm{km\,s^{-1}\,Mpc^{-1}}$.

2 DATA

We have used the high-resolution near-infrared *HST* WFC3/IR data from the CANDELS multicycle treasury programme (Grogin et al. 2011; Koekemoer et al. 2011) centred on the UKIRT Infrared Deep Sky Survey Ultra Deep Survey (UKIDSS UDS; Lawrence et al. 2007) and the Cosmological Evolution Survey (COSMOS; Koekemoer et al. 2007; Scoville et al. 2007) fields. Both the CANDELS UDS and COSMOS near-IR data comprise 4 × 11 WFC3/IR tiles covering a total area of 187 arcmin^2 in each field, in both the $F125W$ and $F160W$ filters with 5σ point-source depths of 27.1 and 27.0 (AB mag), respectively. In addition to near-IR data, we have also made use of the accompanying CANDELS *HST* Advanced Camera for Surveys (ACS) parallels in the $F814W$ and $F606W$ filters (hereafter i_{814} and v_{606}). The 5σ point-source depths are 28.4 for both the i_{814} and v_{606} bands in UDS and 28.5 in COSMOS. Approximately 80 per cent of the area of the UDS and COSMOS fields is covered by both ACS and WFC3 pointings.

2.1 Supporting multiwavelength data

In addition to the near-IR and optical imaging provided by *HST*, we have also utilized the multiwavelength data sets available in each field to constrain SED fitting and determine the physical properties for the galaxies in our sample. For the UDS, these include: Canada–France–Hawaii Telescope (CFHT) u'-band imaging; deep optical *B*-, *V*-, *R*-, i'- and z'-band imaging from the Subaru *XMM–Newton* Deep Survey (SXDS; Sekiguchi et al. 2005; Furusawa et al. 2008); *J*-, *H*- and *K*-band United Kingdom Infrared Telescope (UKIRT) WFCAM imaging from Data Release 8 of the UKIDSS UDS; and *Spitzer* 3.6 μm, 4.5 μm IRAC and 24 μm MIPS imaging from the SpUDS legacy programme (PI Dunlop). For COSMOS, they include: optical imaging in u', g', r', i' and z' bands from MegaCam Canada France Hawaii Telescope Legacy Survey-Deep Field 2 (CFHTLS-D2); z' band from Subaru; *Y*, *J*, *H* and *Ks* from UltraVISTA (PI Dunlop); and *Spitzer* 3.6 μm, 4.5 μm IRAC and 24 μm MIPS imaging from the S-COSMOS survey (PI Sanders).

2.2 Sample selection

We have adopted the sample of Bruce et al. (2014), which comprises a refined sub-sample from the $1 < z_{\rm phot} < 3$ and $M_* > 10^{11}\,{\rm M}_\odot$ CANDELS UDS sample of Bruce et al. (2012) (now making use of an updated stellar-mass fitting technique) and a similarly selected sample in the CANDELS COSMOS field. Photometric redshifts were estimated using a code based on HYPERZ from Bolzonella, Miralles & Pelló (2000), following Cirasuolo et al. (2007) and were subsequently used to determine stellar-mass estimates. The stellar-mass estimates were based on the Bruzual & Charlot (2003) models with single-component exponentially decaying star formation histories with e-folding times in the range $0.3 \leq \tau\,({\rm Gyr}) \leq 5$ and with a minimum model age limit of 50 Myr. Our final sample contains 205 galaxies in the UDS and 191 galaxies in COSMOS with $1 < z_{\rm phot} < 3$ and $M_* > 10^{11}\,{\rm M}_\odot$. As the sample sizes and areas in the UDS and COSMOS fields are comparable and there is good agreement between the comoving number densities of the two fields (Bruce et al. 2014), in the following sections the science results are based on the combined UDS and COSMOS sample unless otherwise stated.

2.3 Star formation rates

Finally, the star formation rates for the UDS and COSMOS samples were estimated from the best-fitting SED models and 24 μm fluxes by adopting the convention of Wuyts et al. (2011), where if any of the objects in the sample have a 24 μm counterpart within a 2 arcsec radius in the SpUDS and S-COSMOS catalogues, their star formation rate is given by ${\rm SFR_{UV+IR}}({\rm M_\odot\,yr^{-1}}) = 1.09 \times 10^{-10}(L_{\rm IR} + 3.3L_{2800})/{\rm L_\odot}$, where $L_{2800} = \nu L_\nu(2800\,{\rm \AA})$ and the contribution to $L_{\rm IR}$ is taken over the wavelength range 8–1000 μm. For objects which do not have 24 μm counterparts, a value of ${\rm SFR_{UV,\,dust\,corrected}}({\rm M_\odot\,yr^{-1}}) = 1.4 \times 10^{-28}\,{\rm L_\nu(erg\,s^{-1}\,Hz^{-1})}$ is adopted (Kennicutt 1998).

For completeness, we have also compared our distinction of passive and star-forming galaxies based on ${\rm sSFR} = 10^{-10}\,{\rm yr^{-1}}$ to those from UVJ colour-cuts following Williams et al. (2009) and found that the two methods agree well.

3 MULTIPLE-COMPONENT MORPHOLOGY FITTING

Following Bruce et al. (2014), the morphologies of the 396 objects in our combined sample have been fitted with both single and multiple-Sérsic light profiles using GALFIT (Peng et al. 2010). This procedure makes use of an empirical point spread function (PSF) generated from a median stack of the brightest (unsaturated) stars in the individual fields (which returns fitted radii consistent to within a few per cent of the sizes fitted using the updated Tiny Tim hybrid CANDELS PSF van der Wel et al. 2012) and adopts a consistent object-by-object background determination (the full effects of which are explored in detail in Bruce et al. 2012), which has been calculated as the median value within an annular aperture centred on each source with an inner radius of 3 arcsec and an outer radius of 5 arcsec. GALFIT is then run on 6 arcsec × 6 arcsec image stamps.

In addition to more basic single-Sérsic light-profile fits, we have also conducted a multiple-component Sérsic light-profile decomposition by fitting two sets of nested models to each object in our sample. The first set of models comprises two single-Sérsic models; one with n = free and the other with n = free + PSF. The second set of nested models includes six multiple-component models. These are: (i) $n = 4$ fixed bulge, (ii) $n = 1$ fixed disc, (iii) $n = 4$ + PSF, (iv) $n = 1$ + PSF, (v) $n = 4 + n = 1$ and (vi) $n = 4 + n = 1$ + PSF, where the PSF is included to account for any centrally concentrated light profile components such as nuclear starbursts or active galactic nucleus. These multiple component models were run with a grid of different initial conditions to ensure that the fitting was robust against the χ^2-minimization routine becoming confined to local minima. The full set-up of initial conditions are listed in Bruce et al. (2012), but in brief include 11 steps in starting magnitudes for the two components ranging from 1, 10, 20 and continuing similarly to 99 per cent of the SEXTRACTOR MAG_AUTO flux in each component, and 21 iterations in the effective radius for each component, which range from 1, 5, 10, 20 to 99 per cent of twice the SEXTRACTOR r_{50} value for each object.

The best-fitting multiple-component models within each of these nested sets were then determined by adopting the simplest model unless a more complex model fit was deemed statistically acceptable, as defined by $\chi^2 \leq \nu + 3\sqrt{(2\nu)}$, and if it satisfied $\chi^2_{\rm complex} < \chi^2_{\rm simple} - \Delta\chi^2(\nu_{\rm complex} - \nu_{\rm simple})$, where ν represents the number of degrees of freedom in the model (in effect the number of parameters), and $\Delta\chi^2(\nu_{\rm complex} - \nu_{\rm simple})$ is the 3σ value for the given difference in the degrees of freedom between the two competing fits. In addition to these criteria, several additional constraints were applied to ensure that the best-fitting models were physically realistic, which included requiring that the flux from a given sub-component

was at least 10 per cent of the total flux of the object, that the axial ratios of the fitted bulge components were not extreme, and that the effective radii of the fitted components did not exceed our fitting radius. This approach provided statistically acceptable multiple-component models for ∼85 per cent of the combined sample and the number of objects which are best fitted by each of the different models is summarized in Bruce et al. (2014) table 2.

3.1 Mock galaxy simulations

In order to estimate the random and systematic uncertainties on our fitted morphological parameters, we have conducted tests using simulated galaxies. Full details of the simulations and accompanying results are presented in Bruce et al. (2014). In summary, we find that we are able to recover B/T ratios to within 10 per cent accuracy for ∼80 per cent of objects, without any significant systematic bias. We also report that component sizes are robust to an accuracy of 10–20 per cent, including systematic errors. However, we note that these are conservative estimates of uncertainties; disc components can be recovered more accurately and there is also a trend for models with smaller component sizes to be fitted with lower random and systematic uncertainties. It should also be noted that the accuracy with which we have been able to determine these fitted parameters relies heavily on the high S/N of the imaging data for our galaxy sample (typically S/N > 50).

We have also utilized the mock galaxy simulations in Bruce et al. (2014) to explore the effects of allowing a PSF component in the fitting. Here, we discuss the cases where our best-fitting single-Sérsic fits have $n > 10$ (with or without a fitted PSF component) in order to ascertain when GALFIT fits these un-physically high values.

Out of 174 of these galaxies, we find that 80 ± 9 per cent have one component with an effective radius of 1 pixel and the other with effective radius 20 pixels (the two extreme sizes modelled). By construction, only 12.5 per cent of *all* our models have this configuration where either the bulge or disc component has $r_{\rm eff} = 1$ and the other component has $r_{\rm eff} = 20$. Within this sub-set 64 ± 4 per cent are from input models where the disc $r_{\rm eff} = 1$ and the remaining 36 ± 4 per cent have bulge $r_{\rm eff} = 1$. Given the relatively small number statistics, it is difficult to make robust statements, but it does not appear that these $n > 10$ fits have any preferential B/T light fraction, axis ratios, relative position angles or an increased probability of being fitted with a single-Sérsic+PSF model. Thus, it appears as though the unphysically high $n > 10$ fits are a result of systems with large differentials in component sizes, which cannot be well fitted with a single Sérsic light profile.

Given that we retain all the single and multiple-component fits, it is also interesting to look at all the models which had an initial single-Sérsic $n > 10$ fit, but where the best fit then adopted a PSF component. Out of 312 of these initial single-Sérsic $n > 10$ fits, 48 ± 5 per cent (151 objects) were then best fitted by Sérsic + PSF, and only 13 objects with these Sérsic + PSF best fits retained an $n > 10$.

Thus, our simulations confirm our assertion (Bruce et al. 2012) that the adoption of the Sérsic + PSF best-fitting models are motivated by the inability of single-Sérsic fits to fully account for multiple components. The significance of the multiple-Sérsic + PSF best-fitting models are discussed in detail in Bruce et al. (2014).

3.2 Extension to additional bands and decomposed SED fitting

Having established H_{160} bulge-disc decomposed morphological fits for all the objects in the combined UDS and COSMOS sample, in Bruce et al. (2014) we were then able to extend this analysis to the other three bands available within CANDELS: J_{125}, i_{814} and v_{606} and conduct separate component SED fitting on the decomposed photometry (where the SED fits were further constrained at the extreme blue and red ends by the overall photometry for the objects). The full details of this procedure are presented in Bruce et al. (2014) and here we highlight that this technique does not rely on the adoption of any functional forms to describe how the morphologies of these massive galaxies vary as a function of redshift, but instead, fixes all morphological parameters at the H_{160}-band best-fitting values. This simplified approach accounts for colour gradients within the bulge + disc systems by allowing the bulge and disc component magnitudes to trade-off against each other and yields realistic colours for the bulge and disc components without any further constraints.

This decomposition technique provides several clear advantages. By providing individual stellar-mass and star formation rates for the separate components (where burst and exponentially decaying star formation history templates with $0.1 \leq \tau\,({\rm Gyr}) \leq 5$ can now be fitted due to the additional degrees of freedom included from the bulge-disc decomposition), we are able to (i) explore the fully decomposed bulge and disc size–mass relations; (ii) study the trends with star formation rate for the separate bulge and disc components, which has provided new insight into the links between quenching and size evolution; (iii) given our $M_* > 10^{11}\,{\rm M}_\odot$ sample selection, the decomposition also allows us to probe the lower mass envelopes of the individual components.

4 RESULTS

4.1 Correlation between single- and multiple-component model morphologies

Having conducted the detailed morphological decomposition described above, and extended this analysis across the four-band wavelength range available from CANDELS, we were then able to compare the overall morphologies fitted by the single-component and the multiple-component fitting techniques. This comparison is shown in Fig. 1, which demonstrates the good correlation between the Sérsic indices fitted from the single-component models and the bulge/total (B/T) light fraction ratios from the H_{160}-band multiple-component decompositions. Overall there is a reasonable correlation between the B/T light fractions from the multiple-component decompositions and the fitted single-Sérsic indices (although there is significant scatter), which are supported by Spearman rank correlation coefficients of 0.87 for the UDS, 0.80 for COSMOS and 0.84 for the combined UDS and COSMOS fields (all with p-values $\ll$0.001). Moreover, the Sérsic index cut at $n = 2$ to distinguish between bulge and disc-dominated galaxies closely corresponds to a cut at $B/T = 0.5$, with only a few cases where galaxies have $n < 2$ and $B/T > 0.5$ or $n > 4$ but $B/T < 0.5$.

In fact, part of the scatter in these correlations can be explained by the fact that the light fractions are plotted as the bulge/total fraction, where the total light can contain contributions from a PSF. In this case, total = (bulge + disc + PSF), which is not the same as bulge + disc light. For comparison, bulge/bulge + disc fractions are plotted in Fig. 2, where objects which have a best-fitting multiple-component model with a PSF component are highlighted in blue. Adopting this bulge/bulge+disc ratio helps to remove some of the scatter towards high Sérsic indices but low bulge fractions and the updated Spearman rank correlation coefficients are 0.88 for the UDS, 0.83 for COSMOS and 0.85 for the combined UDS and

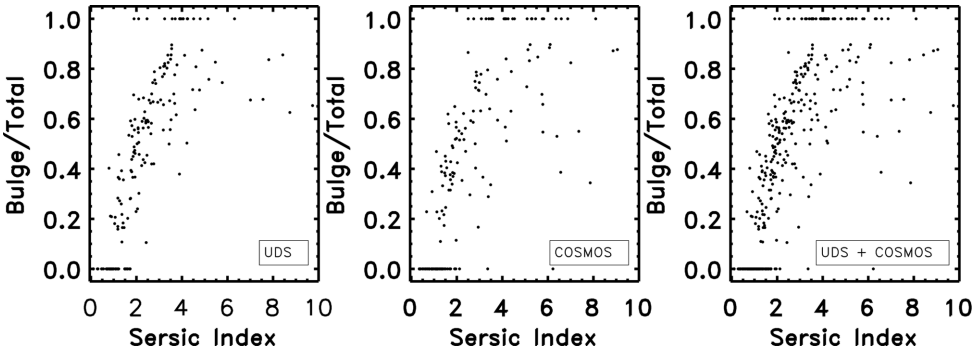

Figure 1. Bulge/Total light fractions against single-Sérsic index fits, split by field. These plots illustrate that the same correlations witnessed in the UDS analysis (Bruce et al. 2012) extend to the COSMOS field, with Spearman rank correlation coefficients of 0.87 and 0.80 for both fields, respectively, and 0.84 for the combined UDS and COSMOS sample, all with p-values $\ll$0.001.

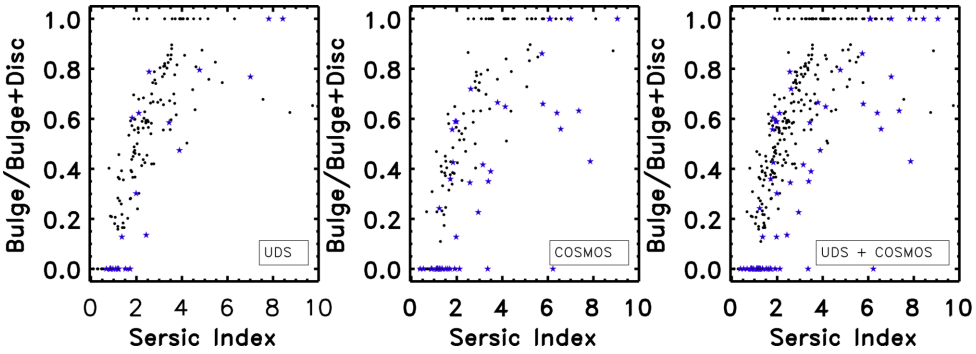

Figure 2. Bulge/Bulge+Disc light fractions from the H_{160}-band modelling against single-Sérsic index fits, with objects which have best-fitting models which contain a PSF component highlighted with blue stars. This demonstrates the same overall trends as in Fig. 1, but here some of the scatter has been reduced and specific cases have been highlighted where the inclusion of a PSF component helps to resolve low $B/B+D$ and high Sérsic index fits.

COSMOS sample, again with p-values $\ll$0.001. In the cases where best fits contained a PSF, the bulge/total ratios fall as the PSF component has replaced some of the contribution which would otherwise be modelled by the bulge, and the Sérsic indices are higher because a simple de Vaucouleurs profile no longer provides an adequate fit to these centrally concentrated objects. Thus, for these systems plotting bulge/bulge+disc light ratios arguably provides a characterization of bulge dominance which is easier to interpret. By highlighting those objects with a significant PSF component (>10 per cent), Fig. 2 also reconciles the single- and multiple-component fits for the two objects which have $B/T = 0$ with $n > 2.5$ as it can now be easily seen that these fits have a PSF component. Hence, whilst they have no bulge component these are not 'pure' disc systems, but have a centrally concentrated light component modelled in the multiple-component analysis by a PSF and in the single-component fits by a high Sérsic index. For completeness, we have also examined the correlation between the B/T mass fractions and $n > 2.5$. In this case, adopting fractions based on stellar-mass estimates generally increases the contribution from the bulge component, as expected given the different stellar populations comprising the bulge and disc components, but otherwise does not lessen the agreement between the single-Sérsic index light-based morphological indicator and the decomposed mass-based discriminator.

The examination of the correlation between single-Sérsic indices and bulge/total H_{160} light fractions and decomposed stellar-mass estimates, confirms that in the majority of cases the single-Sérsic index discriminator at $n = 2.5$ describes the overall morphologies of these most massive galaxies relatively well, as it provides a good proxy for both light- and mass-based measures of $B/T = 0.5$.

4.2 Size–mass relations

The results from the multiple-component decomposition have allowed us to explore how the size–mass relations for the separate bulge and disc components evolve with redshift by accurately decomposing their masses from the multiple-component SED fitting. However, before this is discussed, it is first interesting to explore how the size–mass relations constructed by splitting the mass of each galaxy into each of its separate components according to their contributions to the H_{160}-band light compare to the results presented in Bruce et al. (2012), which used the CANDELS UDS sample alone. The combination of the UDS and COSMOS samples is plotted in Fig. 3 and, following the convention in Bruce et al. (2012), these plots show the size–mass relations for all bulge components in the top panels and disc components in the bottom panels. They are further split by redshift, where the full redshift range ($1 < z < 3$) is displayed in the far left-hand panels, $1 < z < 2$ in the middle and $2 < z < 3$ in the right-hand panels. The bulge relations have been overplotted with the local Shen et al. (2003) ETG relation in red, with its 1σ scatter, and the disc components by the local late-type galaxy (LTG) relation in blue and its scatter, where these relations have been corrected to un-circularized values following the prescriptions outlined in Bruce et al. (2012). In these plots, we only display components with $M_* > 2 \times 10^{10}\,\mathrm{M}_\odot$, as below this mass the components become sufficiently faint that they may introduce potential biases to the morphological properties fitted, therefore they have been removed from these plots to avoid overinterpretation of sub-components.

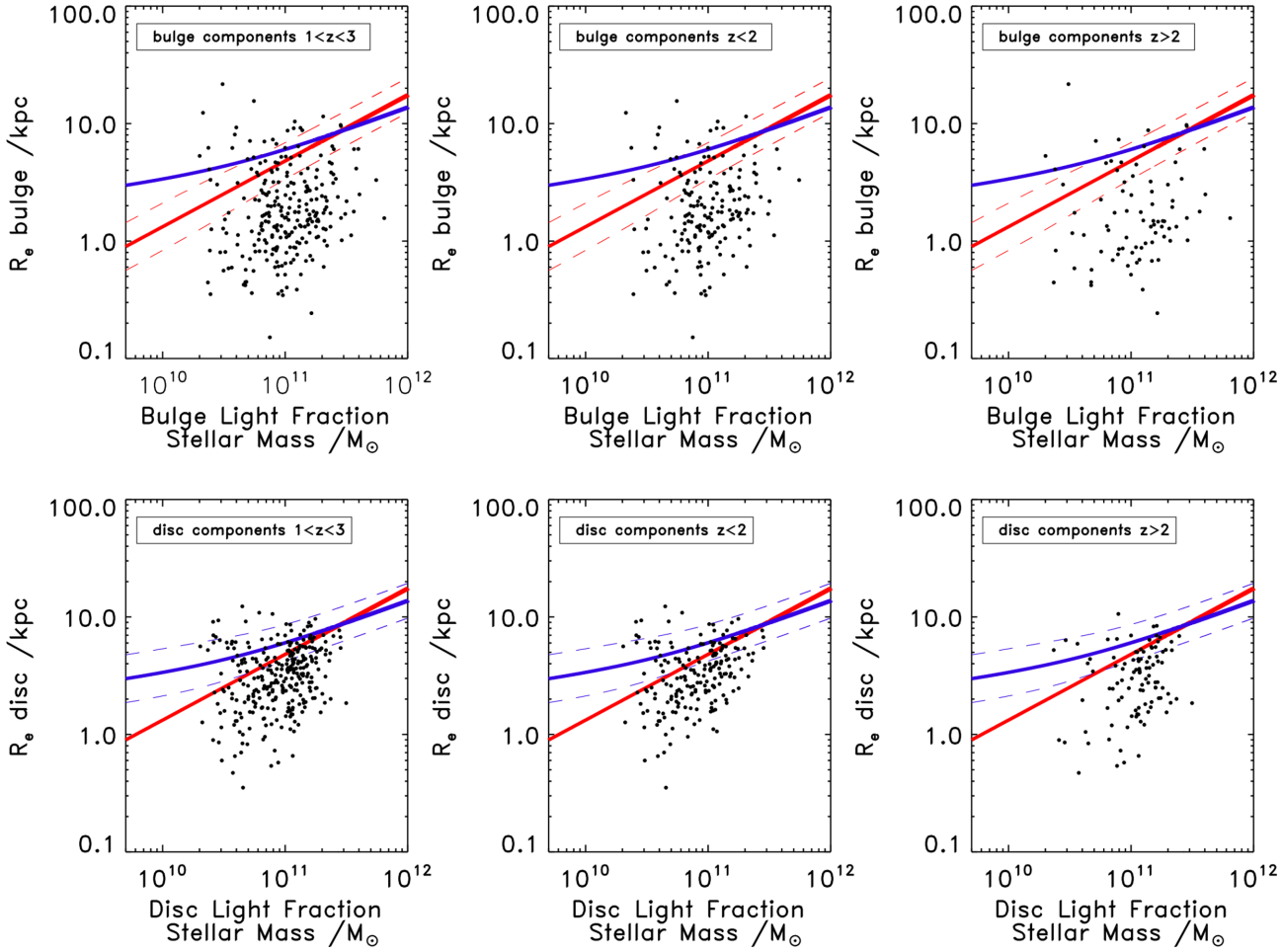

Figure 3. Combined UDS + COSMOS size–mass relations for each component, where component masses are determined based on the H_{160}-band light fractions. For the bulge components, the local (un-circularized) ETG relation from Shen et al. (2003) has been overplotted in red with its 1σ scatter, and for the disc components the local LTG relation has been overplotted in blue.

It is clear from Fig. 3 that the trends reported for the UDS sample are also in place in the COSMOS field, where again we find that the bulge components of massive galaxies display a stronger size evolution with redshift than the disc components. The majority of bulge components have sizes which place them well below their corresponding local relation, whereas the disc components show a smaller scatter in size with an increased fraction of discs displaying sizes consistent with similarly massive local systems. These results also support the claim of a lower envelope of sizes which scales with mass broadly parallel to the local relation.

The scatter in the size–mass relation of the bulge and disc components is higher than it would be expected from the estimated uncertainties in our size and mass measurements, thus implying a significant intrinsic scatter.

We now move on to consider the size–mass relations based on the separate component masses estimated from the SED fitting. These results are presented in Fig. 4. Comparison between these size–mass relations and those plotted in e.g. Fig. 3 reveals no significant change in the reported relations for either the bulge or disc components. This suggests that the simplified approach of attributing masses to each component based on their contributions to the H_{160}-band light fractions provides, at least on average, a good proxy for the SED-fitted stellar-mass decompositions.

This stellar-mass decomposition confirms all of the morphological trends revealed by the previous light-fraction-decomposed size–mass relations, including the stronger evolution witnessed for bulge components over discs, both in terms of the number of bulges which fall below their respective local relations, and in the median sizes of the populations in both the $z < 2$ and $z > 2$ redshift bins. These results are summarized in Table 1, which shows that, within the errors, these trends are consistent across both fields, and are in agreement with the statistics quoted in Bruce et al. (2012) for the size–mass relations from masses based on H_{160}-band light fractions for the UDS field alone. Again, the uncertainties on these values do not allow us to draw any robust conclusions about the change in these fractions with redshift, although we do note that the CANDELS-COSMOS sample contains a larger number of bulge-dominated objects at $z > 2$ which is responsible for the rise of bulges with sizes comparable to local ETGs within this redshift bin. This could be produced by a systematic error (focusing) in the determination of the photometric redshifts. However, the effects of redshift focusing have been studied in both fields with the (albeit low numbers of) spectroscopic redshifts available, but we find no strong evidence for this effect amongst the bulges and conclude that this larger abundance of high-redshift bulges in the CANDELS-COSMOS field may be due to an interception of genuine structure

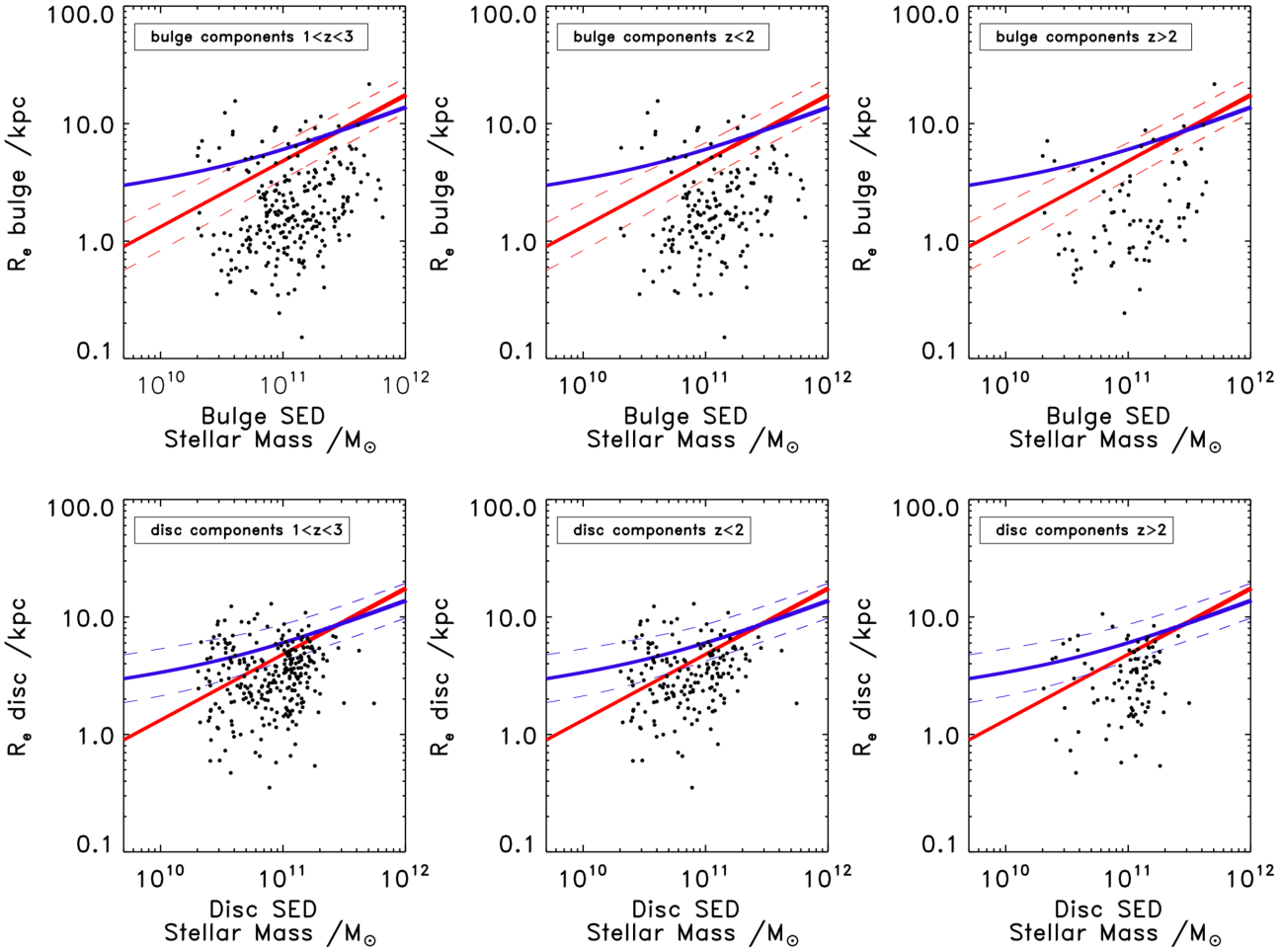

Figure 4. Combined UDS + COSMOS size–mass relations for each component, where now component masses are estimated from the multiple-component SED fitting. The same trends in the sizes of the components witnessed for the relations constructed using masses split according to the H_{160}-band light fractions are also displayed by these relations, which adopt the more robust decomposed SED-fitted component masses. This includes the larger fraction of bulge components which lie below the local relation and the smaller median sizes compared to the disc components, in addition to the lower envelope of sizes displayed. The local ETG relation has again been overplotted in red with its 1σ scatter for comparison with the bulge components, and for comparison with the disc components the local LTG relation has been overplotted in blue.

Table 1. The fractions of components which lie on (or above) their respective local relations within the 1σ scatter and below the 1σ scatter of their relations, where masses for each component have been estimated separately from the multiple-component SED fitting.

		$1 < z < 3$	$1 < z < 2$	$2 < z < 3$
COSMOS	bulges on	21 ± 4 per cent	14 ± 4 per cent	36 ± 8 per cent
	bulges below	79 ± 4 per cent	86 ± 4 per cent	64 ± 8 per cent
	discs on	35 ± 4 per cent	39 ± 5 per cent	25 ± 8 per cent
	discs below	65 ± 4 per cent	61 ± 5 per cent	75 ± 8 per cent
UDS	bulges on	15 ± 3 per cent	16 ± 4 per cent	12 ± 5 per cent
	bulges below	85 ± 3 per cent	84 ± 4 per cent	88 ± 5 per cent
	discs on	56 ± 4 per cent	59 ± 5 per cent	52 ± 6 per cent
	discs below	44 ± 4 per cent	41 ± 5 per cent	48 ± 6 per cent
Combined	bulges on	18 ± 2 per cent	15 ± 3 per cent	23 ± 5 per cent
	bulges below	82 ± 2 per cent	85 ± 3 per cent	77 ± 5 per cent
	discs on	47 ± 3 per cent	49 ± 4 per cent	43 ± 5 per cent
	discs below	53 ± 3 per cent	51 ± 4 per cent	57 ± 5 per cent

in the COSMOS field (although no obvious spatial clustering of these objects is seen).

From this discussion, it is evident that the adoption of the more rigorous SED-decomposed component masses, over the H_{160}-band light fraction mass decompositions, has not significantly influenced the positions of components in their respective size–mass relations, nor altered the basic trends reported. However, the full SED stellar-mass decomposition not only provides robust individual

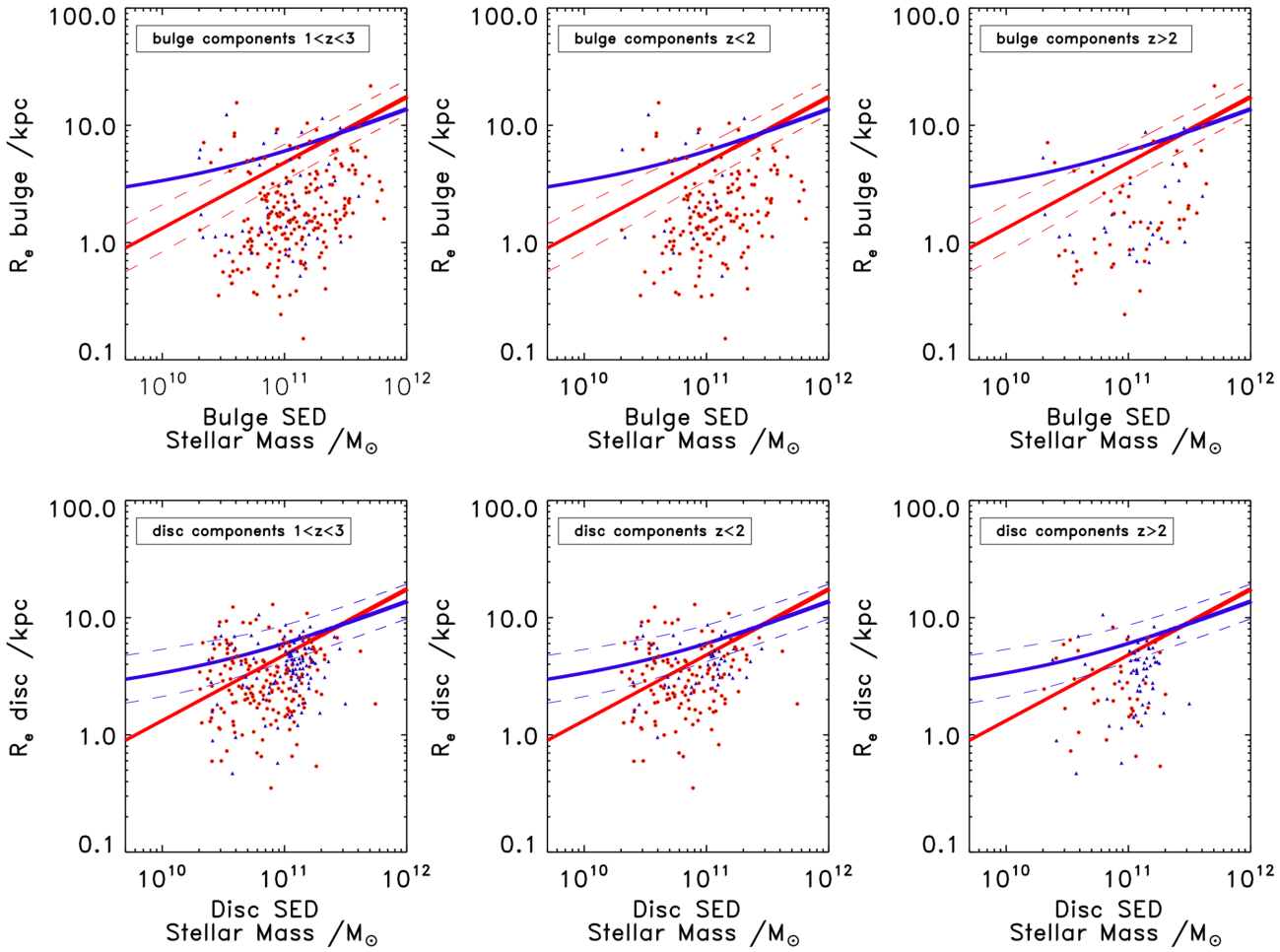

Figure 5. Combined UDS + COSMOS size–mass relations for each component, where component masses are estimated from the multiple-component SED fitting and components are coloured by their star-formation activity using the sSFR $< 10^{-10}\,\mathrm{yr}^{-1}$ limit for passivity (red circle are passive components and blue triangles are star-forming components), and based on the separate component sSFRs from the multiple-component SED fitting. These coloured relations do not reveal a clear division in the sizes of passive and star-forming components, but instead show that the star-forming and passive bulges have comparable sizes with some of the largest bulges being passive and some of the most compact bulges displaying evidence of on-going star formation.

component masses, but also delivers estimates of the star formation activity of each object.

4.3 Star formation trends

Early size–mass studies (e.g. Kriek et al. 2006; Toft et al. 2007) reported a correlation between compactness and passivity which has since gained substantial support in the literature, but these studies are not only limited to morphological classifications based on the single-Sérsic index fits but also [with the exception of integral field unit (IFU) spectroscopic studies] global star formation rates. In this respect, the advantage of our full SED multiband decomposition technique becomes clear, as it has allowed us to estimate the star formation rate (SFR) for each individual bulge and disc component.

In Fig. 5, we now show the size–mass relations plotted with the SED-fitted decomposed stellar masses are now coloured by their individual component star formation rates, where for simplicity we have adopted the sSFR $= 10^{-10}\,\mathrm{yr}^{-1}$ discrimination between star-forming and passive components and plot the passive components in red and the star-forming components in blue. These size–mass plots, containing separate component star formation information, are shown in Fig. 5. These plots do not immediately display a clear division between the sizes of passive and star-forming components, but instead reveal that a fraction of the most compact bulges and discs display signs of continued star formation, while some of the largest bulges and discs are classified as passive. The evolution of bulge and disc components split into their star-forming and passive populations is studied in more detail in the following section by exploring how the median sizes of each sub-population, given as a fractional size of their local counter-parts, evolve with redshift.

4.4 Fractional size evolution

In order to better explore the evolution of bulge and disc components split into their star-forming and passive populations, the fractions of each population which display sizes consistent with or below their respective local relations are given in Table 2, along with the offsets of the median sizes of these populations from their local relations in Table 3. For clarity, all bulges have been compared with the local ETG relation, and discs with the local LTG relation (Shen et al. 2003).

These results reveal that the sizes of passive and star-forming bulges are consistently compact, within the errors, and that star-forming discs are significantly larger. However, they also show

Table 2. The fractions of the combined UDS and COSMOS sample components which lie on or below their respective local relations, where masses for each component have been estimated separately from the multiple-component SED fitting, split further into their star-forming and passive populations using the individual component sSFRs.

	$1 < z < 3$	$1 < z < 2$	$2 < z < 3$
Sf bulges on	29 ± 7 per cent	40 ± 13 per cent	23 ± 8 per cent
Sf bulges below	71 ± 7 per cent	60 ± 13 per cent	77 ± 8 per cent
Sf discs on	48 ± 5 per cent	54 ± 7 per cent	42 ± 7 per cent
Sf discs below	52 ± 5 per cent	46 ± 7 per cent	58 ± 7 per cent
Passive bulges on	15 ± 2 per cent	13 ± 3 per cent	23 ± 6 per cent
Passive bulges below	85 ± 2 per cent	87 ± 3 per cent	77 ± 6 per cent
Passive discs on	46 ± 4 per cent	46 ± 4 per cent	45 ± 8 per cent
Passive discs below	54 ± 4 per cent	54 ± 4 per cent	55 ± 8 per cent

Table 3. The fractional offsets of the median sizes of each population from their respective local relations.

	$1 < z < 3$	$1 < z < 2$	$2 < z < 3$
Bulge components	3.09 ± 0.20	2.93 ± 0.32	3.41 ± 0.58
Star-forming bulges	2.81 ± 0.64	1.83 ± 0.30	3.81 ± 1.0
Passive bulges	3.01 ± 0.19	3.00 ± 0.14	3.24 ± 0.44
Disc components	1.77 ± 0.10	1.65 ± 0.14	1.99 ± 0.25
Star-forming discs	1.62 ± 0.15	1.50 ± 0.13	1.78 ± 0.20
Passive discs	1.94 ± 0.25	1.72 ± 0.27	2.35 ± 0.41

that passive discs have intermediate sizes, larger than their passive bulge counterparts, but smaller than the discs which remain active. To better explore these results, we have calculated the sizes of these sub-divided populations as a fraction of the present-day sizes of similarly massive galaxies, using the median fractional sizes of all objects. This assumes that the slope of the size–mass relation is constant over $0 < z < 3$ (e.g. McLure et al. 2013; van der Wel et al. 2014). These fractional sizes for the bulge and disc components from the full SED-fitting decomposition are shown in Fig. 7. This confirms the trends determined from the size–mass relation plots, but also allows for a more direct and intuitive comparison of component sizes split into star-forming and passive populations at different redshifts. In Fig. 6, we have also included the fractional size evolution as determined from the single-Sérsic fitting, as all previous $1 < z < 3$ light-profile fitting size–mass studies have relied on this parameter to distinguish between bulge and disc-dominated systems. Thus, it allows not only a direct comparison with previous literature results, but also with the multiple-component SED-fitting decomposition results and so serves to highlight the additional insight which can be gained from adopting the decomposition method for galaxy size measurements.

Starting with Fig. 6 for the single-Sérsic fitting technique, where disc-dominated galaxies are classified as $n < 2.5$ following the convention of Shen et al. (2003) and bulges as $n > 2.5$, we found that the size of passive bulges, passive discs and active bulges are all consistent within their errors and are similarly compact, but that star-forming discs are significantly larger. This can clearly be seen in Fig. 6, where we have overplotted as the dotted line the size evolution for ETGs as fitted by van der Wel et al. (2008), given by $R_e(z)/R_0 \propto (1+z)^{-1}$, and as the dashed line the fitted size-evolution of the decomposed star-forming discs (top-right panel of Fig. 7), as given by $R_e(z)/R_0 \propto (1+z)^{-0.5}$.

These trends are consistent with previous studies such as McLure et al. (2013), but raise questions over the mechanisms by which star-

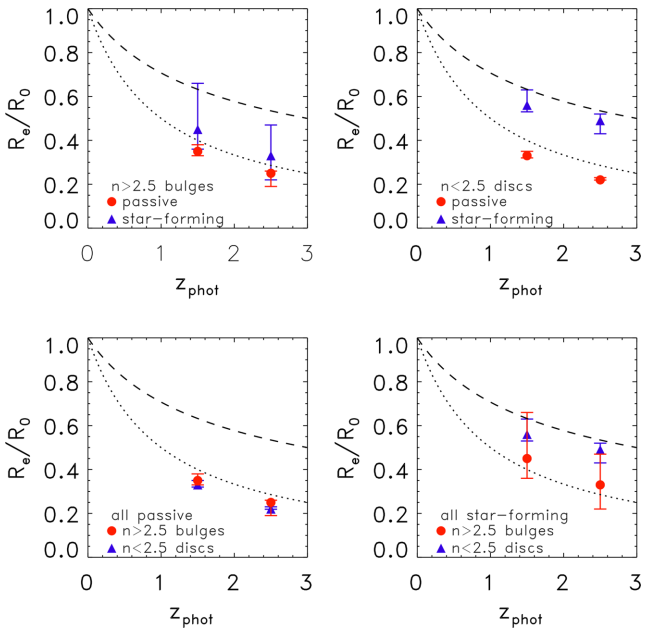

Figure 6. The fractional size evolution of galaxies classified as ETGs and LTGs based on a cut at $n = 2.5$ for our single-Sérsic index fits. The top panels are split into all ETGs (left) and all LTGs (right), whereas the bottom panels show all passive galaxies (left) and all star-forming galaxies (right) to allow an easier comparison of the same data depending on the morphological or star formation activity distinctions. Overplotted as the dotted line is the fitted $R_e(z)/R_0 \propto (1+z)^{-1}$ ETG size evolution from van der Wel et al. (2008), and the dashed line is the relation fitted to our decomposed star-forming disc sample (top-right panel of Fig. 7) given by $R_e(z)/R_0 \propto (1+z)^{-0.5}$. Using the single-Sérsic fits, the passive discs are as compact as star-forming and passive bulges, and are significantly smaller than the sizes of star-forming discs. The sizes of the passive and star-forming bulges are equally compact within the errors, and despite the larger uncertainties, this trend remains for the multiple component SED decompositions represented in Fig. 7.

forming galaxies quench and also significantly reduce in size to form the passive-disc population. One possible reason for this apparent discrepancy may be that the passive-disc galaxies are more bulge dominated than the star-forming discs, and are therefore biased to smaller sizes in this comparison.

In order to test this, we have explored the Sérsic index distributions of both the passive and star-forming discs and do find that using a cut at $n = 2.5$, the passive discs are centred on a higher n values than the star-forming discs. As a result, we have experimented with decreasing the Sérsic index value used as the

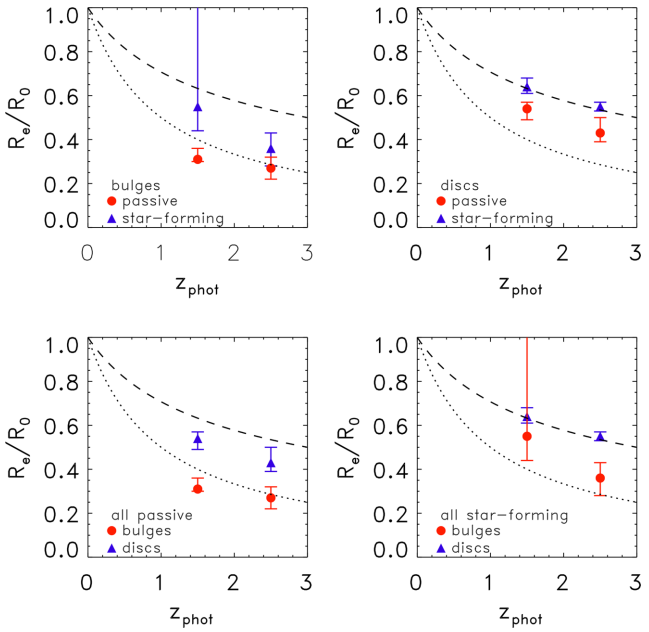

Figure 7. The fractional size evolution of all the bulge and disc components with respect to their local relations in the top-left and right-hand panels, respectively, and for all passive and star-forming components in the bottom-left and right-hand panels. In this case, star-forming and passive discs have been compared to the local LTG relation and star-forming and passive bulges have been compared to the local ETG relation. Overplotted as the dotted line is the fitted $R_e(z)/R_0 \propto (1+z)^{-1}$ ETG size evolution from van der Wel et al. (2008), and the dashed line is the relation fitted to our decomposed star-forming disc sample (top-right panel) given by $R_e(z)/R_0 \propto (1+z)^{-0.5}$. Using the multiple-component SED decompositions, the passive and star-forming bulges arguably remain equally compact within the large errors, but passive discs display an intermediate size as they are larger than their bulge counterparts but smaller than the star-forming discs.

discriminator between bulges and discs, in an attempt to ensure that in order to be classified as passive discs these galaxies are as disc dominated as possible. By decreasing the Sérsic index cut to $n = 2$ and $n = 1.5$, we find a better agreement between the Sérsic index distributions for the passive and star-forming discs (although the passive discs are still centred on slightly higher values of n), but this does not affect the derived fractional sizes of this population. Thus, from the single-Sérsic fitting technique one would always find that the star-forming discs are substantially larger than the passive discs, and in fact that the passive discs have sizes comparable to the star-forming and passive bulges.

Adopting the multiple-component SED-fitting decompositions yields the fractional size evolutions displayed in Fig. 7, which have again been overplotted with the van der Wel et al. (2008) ETG ($R_e(z)/R_0 \propto (1+z)^{-1}$) and the fitted star-forming disc ($R_e(z)/R_0 \propto (1+z)^{-0.5}$) relations. This shows similar size evolution for the bulge components and star-forming discs, but now reveals that the passive discs now have an intermediate size, between the passive and star-forming bulges and the star-forming discs.

It is possible that the inclusion of all passive disc components in this sample introduces some effects associated with the lower masses that are being probed, as for the single-Sérsic index fits all bulges or discs have stellar masses $M_* > 10^{11}\,\mathrm{M}_\odot$, but the decomposed component masses can range as low as $M_* = 2 \times 10^{10}\,\mathrm{M}_\odot$. For these low-mass components, we then compared their sizes to similarly massive local galaxies via the Shen et al. (2003) LTG relation, but in this case we are comparing the size of a low-mass disc component of a much more massive bulge-dominated galaxy to a low-mass disc-dominated system at low redshift, which may bias the fractional size measurements of these galaxies to higher values. However, to account for this we examined these relations using only the bulge component of bulge-dominated galaxies and the disc component of disc-dominated galaxies. Whilst the adoption of this sub-set does not significantly affect the fractional sizes of the bulges or star-forming discs, it does reduce the size of the passive discs, although not by an amount which makes them consistent with the $n < 2.5$ single-Sérsic index passive galaxies. Hence, even though there may be some effect from low-mass sub-components which drives the passive discs to larger sizes, it is not the dominant reason for the increase in passive disc sizes from the multiple-component SED-fitting decomposition, and we are left to conclude that the more accurate decomposition of both individual component stellar-masses and star formation rates reveals a potential bias in the results from the single-Sérsic index fitting technique, with passive disc components genuinely having an intermediate size.

5 DISCUSSION

5.1 Comparison to results in the literature

Despite the profusion of morphological studies of massive $z > 1$ galaxies over the past 5–10 years, these studies have adopted a number of different selection criteria and are often biased towards selecting passive or early-type systems. As a result, it has been difficult to disentangle the trends for galaxies with early-type (ETG) morphologies to be more compact than late-type (LTG) systems, and for passive galaxies to be more compact than those which display on-going star-formation. In order to conduct a robust and direct comparison between the size evolution of bulge- and disc-dominated galaxies, sub-divided further into their passive and star-forming populations, it is important to adopt an unbiased, mass-selected sample, as has been done for this work. Here, we limit comparison of our results to several of the most notable studies which have well-defined samples and stellar-mass and size determination procedures most directly comparable with our own.

We first draw a comparison between our single-Sérsic fits and the study of Buitrago et al. (2008) conducted at $2 < z < 3$ for 82 $M_* > 10^{11}\,\mathrm{M}_\odot$ galaxies with Near Infrared Camera and Multi-Object Spectrometer (NICMOS) *HST* imaging. In this study, Buitrago et al. split their sample into bulge- and disc-dominated systems using a Sérsic index cut at $n = 2$ and find that, on average: the $n < 2$ discs have a fractional size $R_e/R_0 = 0.38 \pm 0.05$; and bulge systems with $n > 2$ have $R_e/R_0 = 0.23 \pm 0.04$. Within the errors, these results are consistent with our $z > 2$ sample using the similarly modelled single-Sérsic fits, where as discussed previously, cutting our sample at the lower $n = 2$ limit does not affect the median fractional sizes that we determine.

We can also compare with the study of McLure et al. (2013) for $M_* > 6 \times 10^{10}\,\mathrm{M}_\odot$, $z = 1.4$ galaxies in the UDS covered in the K band by UKIDSS UDS, and with spectra from FORS2. McLure et al. (2013) split their mass-selected sample by both morphology, above and below $n = 2.5$, and in terms of the overall galaxy star formation activity. They report that, at this redshift, $n < 2.5$ discs have a median $R_e/R_0 = 0.465 \pm 0.032$ and $n > 2.5$ bulges have $R_e/R_0 = 0.42 \pm 0.05$. Whereas, splitting by star formation activity, their passive galaxies have a median $R_e/R_0 = 0.42 \pm 0.035$ and the star-forming sample have a median $R_e/R_0 = 0.625 \pm 0.078$.

McLure et al. (2013) comment that the apparent difference in size between their star-forming and $n < 2.5$ disc samples may be

due to the contribution of a significant fraction of passive discs to the median size offsets. In comparison, both our $z < 2$ single-Sérsic and multiple-component fits are roughly consistent with the results from this study, although we note that the fractional sizes of the McLure et al. (2013) star-forming and passive samples are more consistent with our multiple-component fits than our single-Sérsic results. This may in part be due to the fact that although McLure et al. adopt the same sSFR $< 10^{-10}\,\mathrm{yr}^{-1}$ passivity criterion, their adoption of 'double-burst' star formation histories during SED fitting, may account for the better agreement between their passive and star-forming fractional size measurements and our decomposed fits (which have also allowed multiple star formation history components for each galaxy).

We next compare our results to the study of Toft et al. (2007), which was among the first to note the correlation between galaxy passivity and compactness. The Toft et al. (2007) study was conducted at $z \approx 2.5$ using *HST* NICMOS and ACS imaging, and classified galaxies as active or passive depending on whether or not the SED fits to the galaxies were better modelled by constant or burst star formation histories, and were then cross-checked with 24 μm data. Toft et al. (2007) report that at $z = 2.5$ passive galaxies have $R_e/R_0 = 0.19 \pm 0.03$ and star-forming galaxies have $R_e/R_0 = 0.45 \pm 0.15$.

Again, these results are broadly consistent with the passive and star-forming fractional size estimates from both our single-Sérsic and decomposed fits within the errors, especially given the different classifications adopted for star-forming and passive galaxies and that the Toft et al. (2007) sample spans a much wider, and lower mass range ($0.4 \times 10^{10} < M_* < 5.5 \times 11^{11}\,\mathrm{M}_\odot$). It should also be noted that the Toft et al. (2007) passive sample has a Sérsic index distribution centred on $n < 4$, with ≈80 per cent of objects being better fitted with $n = 1$ rather than $n = 4$ light profiles.

Finally, in order to complete the literature comparison we consider the study of Cimatti et al. (2008) at $1.4 < z < 2$ for a spectroscopically confirmed passive Galaxy Mass Assembly Ultra-Deep Spectroscopic Survey (GMASS) sample imaged with *HST* NICMOS and ACS. Cimatti et al. (2008) split their sample into two redshift bins and report that at $z = 1.6$ their passive galaxies have a median $R_e/R_0 = 0.37 \pm 0.08$ and at $z = 2.5$ $R_e/R_0 = 0.29 \pm 0.14$. Again, these results are in general agreement with our single-Sérsic fits, but in this case, as to some extent with the study of Toft et al. (2007), a departure between the size of passive discs and those of the passive bulges begins to become more apparent.

From this comparison with previous studies which have split their sample according to (or various combinations of) (i) $n = 2$; (ii) $n = 2.5$; (iii) photometrically or spectroscopically determined star formation rates, there is clear evidence for the trends for (i) passive galaxies at any redshift to be more compact than star-forming galaxies, (ii) ETGs ($n > 2.5$) at any redshift to be more compact than LTGs ($n < 2.5$); (iii) star-forming galaxies to display a shallower size evolution with redshift than passive galaxies. However, the intermediate sizes of passive discs only become fully apparent from the morphological decompositions presented in this work.

As a consequence, this suggests that compactness may correlate with some combination of passivity *and* the presence of a significant bulge component in the galaxy.

5.2 Insights into galaxy evolution

By extending our multiple-component light-profile fitting to multi-band photometry and SED fitting to provide individual component masses and star formation rates, we have directly shown that the median sizes of passive discs are smaller than those of star-forming discs, which raises questions of how these star-forming discs evolve into the passive population. In order to better understand this evolution, it is important to note that it is not necessarily physically meaningful to compare the sizes of passive and star-forming discs at the same redshifts. In a secular evolution scenario, we expect the star-forming discs to evolve into the passive population, therefore it is more meaningful to compare the star-forming discs at higher redshifts to passive discs at lower redshifts. In order to conduct this comparison, we have used the SED fits of the passive discs to reverse engineer their fitted star formation histories back to the point at which they would last be classified as star forming, given our sSFR $> 10^{-10}\,\mathrm{yr}^{-1}$ criterion, and determine the time that the component has been quenched as the difference between the age of the galaxy at the best-fitting redshift and the time when it was last active. We find that the median time since these components would last be classified as star forming is 0.8 Gyr before the epoch of observation. Therefore, in order to best compare between the sizes of passive discs and their star-forming progenitors, the comparison should be conducted between passive discs at their current redshift and star-forming discs at redshifts which correspond to ∼1 Gyr earlier. This is shown in Fig. 8, where the fitted $r_e \propto (1 + z)^{-0.5}$ star-forming disc relation has been re-plotted for redshifts corresponding to ∼1 Gyr earlier and can be directly compared to the sizes of the passive discs. From this plot, it can be concluded that the sizes of the passive discs at $1 < z < 3$ are consistent with their star-forming progenitors. It is also worth noting that the most recently quenched discs, (last active <0.5 Gyr earlier), have a median size of $2.47^{+0.28}_{-0.2}$ kpc, which is larger than the median of $1.94^{+0.09}_{-0.14}$ kpc for the whole passive disc population. This lends further support to the assertion that the size offset between the passive and star-forming discs can be accounted for by the relation between size and the redshift of quenching.

The distributions of the masses in the disc components of these disc-dominated passive galaxies and their star-forming progenitors

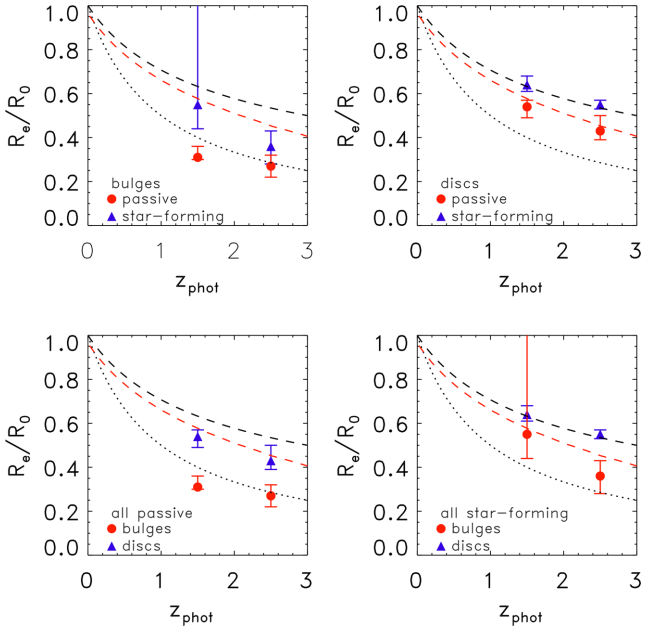

Figure 8. Fractional bulge and disc component size evolution now overplotted in the dashed red line by the relation for the progenitors of the passive discs to allow direct comparison between the sizes of the passive discs and their 1Gyr earlier star-forming progenitors.

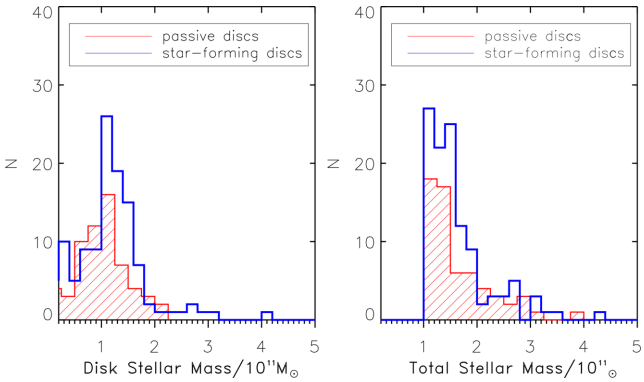

Figure 9. The distribution of the disc component (left) and total (right) masses for the passive and star-forming disc-dominated galaxies. While the disc component masses have a probability $p = 0.06$ of being drawn from the same distribution, with the star-forming progenitors appearing to have a distribution centred on higher masses, the total galaxy masses for these passive and star-forming disc-dominated systems are more comparable with $p = 0.66$. This is consistent with the secular quenching scenario as the evolution of these systems may be accompanied by a transfer of mass from the disc to the bulge components, which would reduce the mass in the disc components but leave the total galaxy mass unchanged.

are shown in Fig. 9, alongside the distributions of the total galaxy masses. The disc component masses of the passive and star-forming discs have a rather low probability of being drawn from the same distribution [$p = 0.06$ from a Kolmogorov-Smirnov (K-S) test], with the star-forming discs appearing to have a distribution centred on slightly higher stellar masses, while the total galaxy mass distributions are more comparable ($p = 0.66$). Any potential evidence for the star-forming disc components being more massive than the passive disc components which they evolve into is in fact consistent with the secular quenching scenario as the evolution of these systems may be accompanied by a transfer of mass from the disc to the bulge components (e.g. Bournaud et al. 2011), which would reduce the mass in the disc components but leave the total galaxy mass unchanged. Whether the processes which quench star formation are secular or merger driven, these observations challenge models to account for this mass evolution and both the presence of massive, quenched discs and their sizes.

When considering the size evolution of all the individual components, it is interesting to address the current claims in the literature that the size evolution of passive galaxies from $z \approx 3$ to the present day can be better explained by the addition of newly quenched, larger galaxies to this population with time (where the size of newly quenched, younger, galaxies scales with the average density of the Universe at the epoch when they quenched) (e.g. Valentinuzzi et al. 2010b; Cassata et al. 2011, 2013; Carollo et al. 2013; Krogager et al. 2013; Poggianti et al. 2013a,b), than by the evolution in size of individual galaxies. One of the natural predictions of this scenario is the star formation-dependent size of *both* bulge and disc components, as at any given epoch the star-forming components are expected to be larger, given the fact that they have not yet quenched but do so at later times. While there is evidence for this trend in the disc components, we do not find strong evidence for a size offset between the passive and active bulges, as has been previously reported by, for example, Carollo et al. (2013), albeit for lower mass systems. However, as discussed in Bruce et al. (2014), the star-forming bulge population is subject to significant contamination from sub-dominant active discs, and the scatter in the sizes of these components is large.

Finally, we discuss the sizes of our passive discs and star-forming bulges within the context of the evolution scenario suggested by Barro et al. (2013, 2014) and Dekel & Burkert (2014). These studies propose that extended star-forming discs at high redshifts first undergo gas-rich dissipational major mergers or experience violent disc instabilities, which both shrink their sizes and transform them from disc to bulge systems, and are then subsequently quenched (with passive bulges later growing in size via e.g. minor mergers). The compact sizes of our star-forming bulges are compatible with this scenario if these systems having undergone disc-bulge transformations, have shrunk, but have not yet quenched. This basic model, which results in size shrinking followed by quenching, by extension, proposes that all quenched systems are equally compact. This can, at least qualitatively, explain the existence and sizes of star-forming bulges, but this is not true for passive discs, which have not undergone morphological or size transformations. This disc population can instead only be explained by secular quenching processes such e.g. halo quenching or ram pressure stripping, which do not transform the underlying morphology *or* sizes of the systems. This further highlights the necessity of models to account for the fact that compactness is here observed to correlate with *both* passivity *and* the presence of a bulge if they are to build a fully consistent scenario.

6 CONCLUSIONS

We have made use of the extended multiple-component bulge + disc morphological decomposition technique presented in Bruce et al. (2014), which allowed us to conduct multiple-component SED fitting and has provided us with stellar-mass and star formation rate estimates for the separate components. By combining these estimates with the decomposed morphological information, we have explored the evolution of the most massive ($M_* > 10^{11}\,\mathrm{M}_\odot$) galaxies at $1 < z < 3$ in terms of the trends witnessed in the size–mass relation and from the median sizes of these systems split by both morphology and star formation activity.

Having conducted this analysis, we have been able to examine the size–mass relations from the combined UDS and COSMOS samples and the relations which utilized the new decomposed stellar-mass estimates, and have found continued evidence that the bulge components display a stronger evolution in the size of the population compared to similarly massive local galaxies than the disc components. This can be seen from both the fraction of bulge components which lie below the local relation and the median sizes of the bulge components split above and below $z = 2$.

We have also found that, at $1 < z < 2$, 15 ± 3 per cent of bulges have sizes consistent with the local ETG relation within its 1σ scatter, with the median bulge component sizes being a factor of 2.93 ± 0.32 smaller than similarly massive local ETGs. At $2 < z < 3$, this fraction of bulges with sizes comparable to the local ETG relation becomes 23 ± 6 per cent and median bulge component size is a factor of 3.41 ± 0.58 smaller than local ETGs. In comparison, at $1 < z < 2$, 49 ± 6 per cent of the disc components have sizes consistent with the local LTG relation and its 1σ scatter, and the median size is a factor of 1.65 ± 0.14 smaller. In the high-redshift bin, these numbers become 43 ± 8 per cent and the median size is a factor of 1.99 ± 0.25 smaller. The scatter in both the bulge and disc relations is larger than the measurement error and thus reflects the intrinsic scatter in the size–mass relations. However, by incorporating the new star formation rate estimates from the

decomposed SED fitting, we do not find a clear distinction in the position of the passive and star-forming components on the size–mass relations.

In order to further explore how the star formation activity correlates with galaxy size, we have examined the sizes of the galaxies in our sample as a fraction of the sizes of local similarly massive galaxies, split into the passive and star-forming bulge and disc subpopulations and plotted above and below $z = 2$. By constructing these samples based on both the $n = 2.5$ single-Sérsic fits with the overall star formation rates, and using the decomposed morphologies and star formation rates, we have highlighted the advantages in decomposing these galaxy properties. This analysis reveals that, the single-Sérsic fits would indicate that the star-forming and passive bulges, and passive discs are equally compact in size with the star-forming discs having larger sizes (although the robustness of the star-forming bulge sample is questionable due to the high level of contamination from star-forming disc components; Bruce et al. 2014). However, the decomposed fits show that the passive discs have intermediate sizes. As the single-Sérsic fractional sizes are in broad agreement with results from previous studies, this clearly demonstrates that adopting the single-Sérsic fits presents a simplified view of the evolutionary processes involved, where for bulge-dominated systems morphology is the main indicator of compactness and for discs the main indicator is star formation. In comparison, the decomposed fits reveal that compactness correlates with some combination of passivity and the presence of a significant bulge component.

Moreover, by assuming that the star-forming discs are the direct progenitors of the passive discs, and by evolving the star formation histories of the passive discs back to the redshifts $\sim$1 Gyr earlier, when the passive discs were still active, we have shown that the passive discs and their star-forming progenitor discs have consistent sizes.

ACKNOWLEDGEMENTS

The authors would like to thank Roberto Abraham, Philip Best and the anonymous referee for their constructive comments, which helped to improve this paper. VAB acknowledges the support of the Science and Technology Facilities Council (STFC) via the award of an STFC Studentship. VAB and JSD acknowledge the support of the EC FP7 Space project ASTRODEEP (Ref. No: 312725). JSD, RAAB, FB and TAT acknowledge the support of the European Research Council via the award of an Advanced Grant. JSD and RJM acknowledge the support of the Royal Society via a Wolfson Research Merit Award and a University Research Fellowship, respectively. RJM acknowledges the support of the Leverhulme Trust via the award of a Philip Leverhulme Research Prize. MC acknowledges the support of the Science and Technology Facilities Council (STFC) via the award of an STFC Advanced Fellowship. US authors acknowledge support from NASA grants for *HST* Program GO-12060. SMF, DCK, DDK and EJM also acknowledge support from NSF grant AST-08-08133.

This work is based in part on observations made with the NASA/ESA *Hubble Space Telescope*, which is operated by the Association of Universities for Research in Astronomy, Inc., under NASA contract NAS5-26555. This work is based in part on observations made with the *Spitzer Space Telescope*, which is operated by the Jet Propulsion Laboratory, California Institute of Technology under NASA contract 1407.

REFERENCES

Allen P. D., Driver S. P., Graham A. W., Cameron E., Liske J., de Propris R., 2006, MNRAS, 371, 2
Barden M., Häußler B., Peng C. Y., McIntosh D. H., Guo Y., 2012, MNRAS, 422, 449
Barro G. et al., 2013, ApJ, 765, 104
Barro G. et al., 2014, ApJ, 791, 52
Belli S., Newman A. B., Ellis R. S., 2014, ApJ, 783, 117
Bolzonella M., Miralles J., Pelló R., 2000, A&A, 363, 476
Bournaud F., Dekel A., Teyssier R., Cacciato M., Daddi E., Juneau S., Shankar F., 2011, ApJ, 741, L33
Bruce V. A. et al., 2012, MNRAS, 427, 1666
Bruce V. A. et al., 2014, MNRAS, preprint (arXiv:1405.1736)
Bruzual G., Charlot S., 2003, MNRAS, 344, 1000
Buitrago F., Trujillo I., Conselice C. J., Bouwens R. J., Dickinson M., Yan H., 2008, ApJ, 687, L61
Buitrago F., Trujillo I., Conselice C. J., Häußler B., 2013, MNRAS, 428, 1460
Cameron E., Driver S. P., Graham A. W., Liske J., 2009, ApJ, 699, 105
Carollo C. M. et al., 2013, ApJ, 773, 112
Cassata P. et al., 2010, ApJ, 714, L79
Cassata P. et al., 2011, ApJ, 743, 96
Cassata P. et al., 2013, ApJ, 775, 106
Cimatti A. et al., 2008, A&A, 482, 21
Cirasuolo M. et al., 2007, MNRAS, 380, 585
Daddi E. et al., 2005, ApJ, 626, 680
Damjanov I. et al., 2009, ApJ, 695, 101
Davari R., Ho L. C., Peng C. Y., Huang S., 2014, ApJ, 787, 69
de Jong R. S., 1996, A&A, 313, 45
Dekel A., Burkert A., 2014, MNRAS, 438, 1870
Fan L., Lapi A., De Zotti G., Danese L., 2008, ApJ, 689, L101
Fan L., Lapi A., Bressan A., Bernardi M., De Zotti G., Danese L., 2010, ApJ, 718, 1460
Franx M., van Dokkum P. G., Schreiber N. M. F., Wuyts S., Labbé I., Toft S., 2008, ApJ, 688, 770
Furusawa H. et al., 2008, ApJS, 176, 1
Grogin N. A. et al., 2011, ApJS, 197, 35
Häussler B. et al., 2007, ApJS, 172, 615
Hopkins P. F., Cox T. J., Younger J. D., Hernquist L., 2009, ApJ, 691, 1168
Kennicutt R. C., Jr, 1998, ARA&A, 36, 189
Khochfar S., Silk J., 2006, ApJ, 648, L21
Koekemoer A. M. et al., 2007, ApJS, 172, 196
Koekemoer A. M. et al., 2011, ApJS, 197, 36
Kriek M. et al., 2006, ApJ, 649, L71
Kriek M., van Dokkum P. G., Franx M., Illingworth G. D., Magee D. K., 2009, ApJ, 705, L71
Krogager J.-K., Zirm A. W., Toft S., Man A., Brammer G., 2013, ApJ, preprint (arXix:1309.6316)
Lackner C. N., Gunn J. E., 2012, MNRAS, 421, 2277
Lang P. et al., 2014, ApJ, 788, 11
Lawrence A. et al., 2007, MNRAS, 379, 1599
Mancini C. et al., 2010, MNRAS, 401, 933
McLure R. J. et al., 2013, MNRAS, 428, 1088
Mortlock A. et al., 2013, MNRAS, 433, 1185
Mozena M., Faber S. M., Koo D. C., Primack J. R., Dekel A., Moody C. E., Ceverino D. CANDELS, 2013, American Astronomical Society, 221, 112
Muzzin A., van Dokkum P., Franx M., Marchesini D., Kriek M., Labbé I., 2009, ApJ, 706, L188
Naab T., Johansson P. H., Ostriker J. P., Efstathiou G., 2007, ApJ, 658, 710
Newman A. B., Ellis R. S., Treu T., Bundy K., 2010, ApJ, 717, L103
Newman A. B., Ellis R. S., Bundy K., Treu T., 2012, ApJ, 746, 162
Peng C. Y., Ho L. C., Impey C. D., Rix H.-W., 2010, AJ, 139, 2097
Poggianti B. M. et al., 2013a, ApJ, 762, 77
Poggianti B. M., Moretti A., Calvi R., D'Onofrio M., Valentinuzzi T., Fritz J., Renzini A., 2013b, ApJ, 777, 125
Scoville N. et al., 2007, ApJS, 172, 1

Sekiguchi K., Akiyama M., Furusawa H., Simpson C., Takata T., Ueda Y., Watson M. W. Sxds Team, 2005, in Renzini A., Bender R., eds, Multiwavelength Mapping of Galaxy Formation and Evolution. Springer-Verlag, Berlin, p. 82
Shankar F., Marulli F., Bernardi M., Mei S., Meert A., Vikram V., 2011, MNRAS, 428, 109
Shen S., Mo H. J., White S. D. M., Blanton M. R., Kauffmann G., Voges W., Brinkmann J., Csabai I., 2003, MNRAS, 343, 978
Simard L., Mendel J. T., Patton D. R., Ellison S. L., McConnachie A. W., 2011, ApJS, 196, 11
Szomoru D. et al., 2010, ApJ, 714, L244
Szomoru D., Franx M., van Dokkum P. G., 2012, ApJ, 749, 121
Taylor E. N., Franx M., Glazebrook K., Brinchmann J., van der Wel A., van Dokkum P. G., 2010, ApJ, 720, 723
Toft S. et al., 2007, ApJ, 671, 285
Trujillo I. et al., 2006, ApJ, 650, 18
Trujillo I., Conselice C. J., Bundy K., Cooper M. C., Eisenhardt P., Ellis R. S., 2007, MNRAS, 382, 109
Trujillo I., Cenarro A. J., de Lorenzo-Cáceres A., Vazdekis A., de la Rosa I. G., Cava A., 2009, ApJ, 692, L118
Trujillo I., Carrasco E. R., Ferré-Mateu A., 2012, ApJ, 751, 45
Valentinuzzi T. et al., 2010a, ApJ, 712, 226
Valentinuzzi T. et al., 2010b, ApJ, 721, L19
van de Sande J. et al., 2011, ApJ, 736, L9
van de Sande J. et al., 2013, ApJ, 771, 85
van der Wel A., Holden B. P., Zirm A. W., Franx M., Rettura A., Illingworth G. D., Ford H. C., 2008, ApJ, 688, 48
van der Wel A., Bell E. F., van den Bosch F. C., Gallazzi A., Rix H.-W., 2009, ApJ, 698, 1232
van der Wel A. et al., 2011, ApJ, 730, 38
van der Wel A. et al., 2012, ApJS, 203, 24
van der Wel A. et al., 2014, ApJ, 788, 28
van Dokkum P. G. et al., 2008, ApJ, 677, L5
Williams R. J., Quadri R. F., Franx M., van Dokkum P., Labbé I., 2009, ApJ, 691, 1879
Wuyts S. et al., 2011, ApJ, 738, 106
Wuyts S. et al., 2012, ApJ, 753, 114

This paper has been typeset from a TEX/LATEX file prepared by the author.